Controls on Fe reduction and mineral formation by a subsurface bacterium

SUSAN GLASAUER,[1,*] PETER G. WEIDLER,[2] SEAN LANGLEY,[1] and TERRY J. BEVERIDGE[1]

[1]Department of Microbiology, College of Biological Sciences, University of Guelph, Guelph, Ontario N1G 2W1, Canada
[2]Forschungzentrum Karlsruhe GmbH, Institute for Technical Chemistry, Water, and Geotechnology Division, Nanomineralogy Group (ITC-WGT), D-76021 Karlsruhe, Germany

Abstract—The reductive dissolution of FeIII (hydr)oxides by dissimilatory iron-reducing bacteria (DIRB) could have a large impact on sediment genesis and Fe transport. If DIRB are able to reduce FeIII in minerals of high structural order to carry out anaerobic respiration, their range could encompass virtually every O_2-free environment containing FeIII and adequate conditions for cell growth. Previous studies have established that *Shewanella putrefaciens* CN32, a known DIRB, will reduce crystalline Fe oxides when initially grown at high densities in a nutrient-rich broth, conditions that poorly model the environments where CN32 is found. By contrast, we grew CN32 by batch culture solely in a minimal growth medium. The stringent conditions imposed by the growth method better represent the conditions that cells are likely to encounter in their natural habitat. Furthermore, the expression of reductases necessary to carry out dissimilatory Fe reduction depends on the method of growth. It was found that under anaerobic conditions CN32 reduced hydrous ferric oxide (HFO), a poorly crystalline FeIII mineral, and did not reduce suspensions containing 4 mM FeIII in the form of poorly ordered nanometer-sized goethite (α-FeOOH), well-ordered micron-sized goethite, or nanometer-sized hematite (α-Fe$_2$O$_3$) crystallites. Transmission electron microscopy (TEM) showed that all minerals but the micron-sized goethite attached extensively to the bacteria and appeared to penetrate the outer cellular membrane. In the treatment with HFO, new FeII and FeIII minerals formed during reduction of HFO-Fe in culture medium containing 4.0 mmol/L P_i (soluble inorganic P), as observed by TEM with energy-dispersive X-ray spectroscopy, selected area electron diffraction, and X-ray diffraction. The minerals included magnetite (Fe_3O_4), goethite, green rust, and vivianite [$Fe_3(PO_4)_2 \cdot 8H_2O$]. Vivianite appeared to be the stable end product and the mean coherence length was influenced by the rate of FeIII reduction. When P_i was 0.4 mol/L under otherwise identical conditions, goethite was the only mineral observed to form, and less Fe^{2+} was produced overall. Hence, the ability of DIRB to reduce Fe (hydr)oxides may be limited when the bacteria are grown under nutrient-limited conditions, and the minerals that result depend on the vigor of FeIII reduction. *Copyright © 2003 Elsevier Science Ltd*

1. INTRODUCTION

The dissimilatory iron-reducing bacteria (DIRB), *Shewanella putrefaciens*, is a facultative anaerobe and substitutes Fe^{3+} for O_2 as the terminal electron acceptor of the electron transport chain to gain energy for growth and metabolism (Nealson and Saffarini, 1994). The organism can reduce Fe(III) (hydr)oxide minerals, including hydrous ferric oxide (HFO), goethite, hematite, and magnetite (Roden and Zachara, 1996; Fredrickson et al., 1998; Zachara et al., 1998), as well as FeIII in natural sediments (Fredrickson et al., 1998) and structural FeIII bound in clay minerals (Kostka et al., 1999). These previous investigations considered Fe reduction under conditions where the composition of the growth medium and the metabolic fitness of the microorganism are optimized to achieve rapid rates of reduction. On the other hand, it is known that the production of cell factors affecting reduction depends strongly on culture conditions, with Fe reduction rates increasing with the level of nutrition (Obuekwe and Westlake, 1982; Arnold et al., 1986b). The rich growth media favored in laboratory experiments may select for traits that enable or enhance reduction of FeIII minerals relative to the often poor nutrition

occurring in natural subsurface environments (Dawes, 1985; Koch, 1985).

In support of these observations, Fe reduction in natural environments has been closely correlated only with the presence of poorly crystalline Fe (hydr)oxides (Munch and Ottow, 1980; Lovley and Phillips, 1986b; Thamdrup and Canfield, 1996; Thamdrup, 2000). There are several explanations for this in addition to nutritional effects. Surface area as well as structural order affect the abiotic and biotic dissolution behavior of minerals (Roden and Zachara, 1996; Weidler et al., 1998; Glasauer et al., 1999), and the size of the crystal may hinder the attachment of cells to minerals (Glasauer et al., 2001). DIRB mediate the formation of Fe mineral phases by delivering Fe^{2+} to the bulk solution after attachment to and reduction of FeIII minerals at the cell surface (Arnold et al., 1986b; Lower et al., 2001), away from the cell via electron shuttling mechanisms (Lovley et al., 1996; Newman and Kolter, 2000), or possibly via soluble cytochromes (Seeliger et al., 1998).

There is evidence that microorganisms can strongly influence Fe mineral cycling (Burdige and Nealson, 1986; Lovley and Phillips, 1986a; Canfield et el., 1993), yet the abiotic formation of Fe minerals has been far more thoroughly studied than mineral transformations mediated by bacteria (Cornell and Schwertmann, 1996). Although the same basic processes of crystal nucleation and growth take place in both biotic and abiotic systems, the formation of minerals in the presence of

* Author to whom correspondence should be addressed (glasauer@uoguelph.ca).

DIRB will depend on the rate at which Fe^{2+} is released from the FeIII phase by bacterial reduction. This implies that the ability of bacteria to reduce Fe, determined by the cells' physiologic status, can be manipulated to affect the mineral formed and its rate of crystallization. Laboratory experiments that achieve fast rates of bacterial Fe reduction through the use of high cell concentrations and the cultivation of cells in nutritionally rich media may mask or eliminate slower mineral-forming processes, and different equilibria are reached (Roden and Zachara, 1996; Fredrickson et al., 1998; Zachara et al., 1998).

Both the dissolution and crystallization of Fe minerals are a function of environmental conditions. Solutes such as phosphate, organic anions, and silicate strongly influence dissolution and nucleation behavior, as well as determine crystal habit (Cornell and Schwertmann, 1979; Mann et al., 1989; Glasauer et al., 1999). Phosphate is of particular interest because it is often limiting to microbial growth in natural aqueous environments (Schindler, 1977; Hudson et al., 2000; Wu et al., 2000). The interplay between cellular P nutrition, Fe reduction and mineral formation has not been well studied.

In addition to expelling metal ions from the cell to form spatially distinct minerals, bacteria can sorb large amounts of metals and form surface precipitates. Bacteria usually have a net negative surface charge at circumneutral pH as a result of acidic functional groups (Beveridge, 1981; Collins and Stotzky, 1992). This makes them highly reactive to positively charged metal species, as demonstrated by studies of metal sorption (Fein et al., 1997; Daughney and Fein, 1998). The reactivity of the cell to metal ions at the bulk aqueous interface has several consequences. Sorption of metals to the outer membrane of gram-negative bacteria and subsequent mineral growth at the surface may compete with mineral formation in the bulk solution, or even disable the cells. Laboratory studies have proven that cells can act as templates for the nucleation of metal precipitates (Langley and Beveridge, 1999), and there is evidence that minerals in natural environments nucleate on cells (Ferris et al., 1986, 1987; Fortin et al., 1998). Fe(hydr)oxide minerals added to cultures of *S. putrefaciens* have a demonstrated high affinity for the cell surface (Glasauer et al., 2001). The location of biomineral precipitates will depend on properties of the metal and the microorganisms, reflecting chemical gradients established between bacteria and the extracellular environment.

Our purpose in this study was to investigate bacterial metal reduction under nutrient-limited conditions that approximate natural subsurface reducing environments where *S. putrefaciens* can be found, to examine the following: (1) the bacterium's ability to reduce hydrous ferric oxides (HFO), goethite, and hematite under slow growth conditions; (2) the association of the initial FeIII minerals and the postreduction minerals with the cell surface; and (3) the influence of the rate of HFO reduction on the minerals that form.

2. MATERIALS AND METHODS

2.1. Fe Minerals

HFO was prepared by rapidly adding 1 mol/L NaOH to 2 mol/L FeCl3 · 6H2O until the pH reached 7 (i.e., the Fe:OH ratio was ~1). The precipitate was washed five times in sterile deionized water.

Analysis by X-ray diffraction (XRD) showed two broad diffraction lines characteristic for HFO (also termed two-line ferrihydrite). Transmission electron microscopy (TEM) revealed strongly aggregated spherical particles ~3 nm in diameter. Conditions for XRD and TEM are described below.

Nanometer-sized crystals of goethite and hematite, and microcrystalline goethite, were prepared by hydrolysis of $Fe(NO_3)_3$ salts. For nanogoethite, $Fe(NO_3)_3 \cdot 9H_2O$ was dissolved in HNO_3, followed by the addition of 1 mol/L NaOH to yield an Fe:OH ratio of 2 and a pH value of 1.8. After 60 d the precipitate was washed three times and dialyzed in sterile deionized water. The microgoethite was prepared by the same method but with an initial Fe:OH ratio of 4 at an initial pH of 12.5. Characterization of these goethite minerals in a previous study by XRD, TEM, Mössbauer spectroscopy, and dissolution experiments showed that the synthesis at pH 1.8 results in pure goethite crystals ~20 nm long (c-axis) with a more disordered structure than the product from the alkaline goethite synthesis (Glasauer et al., 1999). Characterization of the alkaline product showed well-crystalline multidomain particles ~800 nm long (Glasauer et al., 1999).

The hematite was prepared according to Hematite Method 1 described by Schwertmann and Cornell (1991), and the product was washed and dialyzed as for the goethite. The synthesis resulted in diamond-shaped crystals 30 to 50 nm in diameter with a surface area of ~30 m^2/g. The mineralogy was confirmed by selected area electron diffraction (SAED). All of the minerals were prepared using sterile techniques and were checked for microbial contamination by plating on trypticase soy agar (TSA; Becton-Dickinson). In addition, the minerals were kept at 4°°C as suspensions and not dried because drying increases the strong aggregation to which nanominerals are prone.

2.2. Bacteria

Cultures of *S. putrefaciens* CN32 were provided by Y. Gorby of the Pacific Northwest National Laboratory in Richland, Washington, USA. Strain CN32 was isolated from a subsurface core sample obtained from the Morrison Formation during drilling of a shale-sandstone sequence in northwestern New Mexico, USA (Zachara et al., 1998). Cells were maintained as frozen cultures from which they were plated on TSA plates to revitalize for the experiments. Single colonies from TSA plates were inoculated into a defined minimal medium broth (DM) consisting of trace element salts, 3.9 mM PO_4^{3-}, 20 mM lactate, and 4.5 mM 1, 4-piperazinediethanesulfonic acid (PIPES) buffer, at pH 6.5 (Fredrickson et al., 1998). Cells were then grown to midexponential phase (OD_{560nm} = 0.2) under aerobic conditions, washed twice with fresh sterile DM, sparged with H_2/Ar (4:96), and reinoculated into flasks containing sterile DM that had been similarly sparged with H_2/Ar and to which sterile suspensions of mineral Fe or fumarate were added to serve as electron acceptors, as described below.

2.3. Reduction of HFO, Goethite, and Hematite

Sterile suspensions of HFO, nanogoethite, microgoethite, or hematite were sparged with H_2/Ar and injected into 100-mL serum bottles containing 60 mL sparged DM to yield [Fe] = 4 mM. Treatments with fumarate were injected with sterile anaerobic fumarate suspension to yield concentrations of 10 mM. Because cell densities were too low in CN32 cultures grown under anaerobic conditions to isolate sufficient cells for inoculation of the medium, bacteria were grown aerobically in DM to mid–late exponential growth phase, centrifuged at 3000 × *g*, and washed three times with fresh sterile DM, sparged with H_2/Ar and then inoculated into the prepared bottles to yield initial cell numbers of around 10^7 colony-forming units (cfu)/mL. All treatments were repeated in triplicate, and cell-free blanks were included. Aliquots were removed at selected time intervals with a sterile syringe and monitored for reduction potential, cell concentration, Fe^{2+}, and total Fe as described below. All experiments and samplings were performed in an anaerobic chamber (Coy Laboratory Products).

2.4. Reduction of HFO and the Formation of New Minerals

Experiments were conducted as described above with 600 mL DM in 1-L serum bottles. Most reports of DIRB reduction are based on results of single experiments; to investigate variation due to the natural and

inevitable variability of biologic organisms, we decided to perform several time-successive replicates. The four treatments (1HFO, 2HFO, 3HFO, and 4HFO) contained 8 to 16 mM HFO-Fe, representative of Fe concentrations in many marine sediments (Thamdrup, 2000). Treatments 1, 2, and 3 were essentially identical and contained 4 mM $NaH_2PO_4 \cdot H_2O$. This [P_i] was chosen to oversaturate the HFO surface with P, given an estimated specific surface area of 500 m^2/g and P site occupancy of 2.5 μmol P/m^2 (Cornell and Schwertmann, 1996). Soluble phosphate has a high affinity for Fe(hydr)oxide surfaces, which can effectively remove it from solution (Cornell and Schwertmann, 1996). Measurements on filtered samples of cell-free DM containing 8 mM HFO-Fe and 4.0 mM $NaH_2PO_4 \cdot H_2O$, and equilibrated for 1 h, showed that 80% of the P_i remained soluble. For 4HFO, $NaH_2PO_4 \cdot H_2O$ was 0.4 mM, undersaturating the HFO surface; P_i was not detected in cell-free flasks of DM with 8 mM HFO. By varying P_i, we hoped to determine the extent to which the bacteria could scavenge phosphate, which is often a limiting nutrient in natural environments, from the mineral. Although the concentrations chosen for the experiments are higher than those common to natural environments (e.g., Hudson et al., 2000; Wu et al., 2000), they were necessary to achieve Fe reduction before total die-off of the culture took place. Treatments 1HFO, 2HFO, and 3HFO were carried out consecutively over 9 months; 4HFO was run concurrently with 3HFO. At the end of the experiment, precipitates were allowed to sediment for 24 h; washed twice with sterile, sparged, and deionized water; and dried in the anaerobic chamber.

2.5. Analyses

Cell concentrations were determined by colony counts on TSA plates. The reduction potentials of suspensions in the anaerobic chamber were measured by electrode measurements (Corning combination electrode). Production of Fe^{2+} was monitored by the ferrozine method (Lovley and Phillips, 1986a) after 24-h extraction of a 0.5-mL aliquot in 4.5 mL 0.5 mol/L HCl; no solids remained in the tube after this time. Extraction of ferrihydrite undergoing bacterial reduction in 0.5 mol/L HCl for at least 1 h removed 86 to 98% of total Fe added as HFO (Fredrickson et al., 1998). We found that extraction in 3 mol/L HCl gave results identical to a 1-d extraction in 0.5 mol/L HCl within experimental error. For the experiment on reduction of HFO, goethite and hematite, total Fe was measured by extraction in 6 mol/L HCl and analysis by atomic absorption spectrophotometry (Glasauer et al., 2001). For the study of mineral formation during HFO reduction, total Fe was measured by hydroxylamine-HCl extraction (Stookey, 1970). Phophate was measured on filtered (0.2 μm) samples via the ammonium paramolybdate method based on ascorbic acid reduction of the ammonium phosphomolybdate complex (Olsen and Sommers, 1982).

Samples for high-performance liquid chromatography were filtered and kept frozen until all samples were ready for measurement. Data were collected after Clarke (1993) with a Beckman Gold instrument with an HPX-87H organic acid column (Bio-Rad Laboratories) and was calibrated for lactate and acetate with freshly prepared standards.

2.6. TEM

Cells and minerals were processed for TEM, energy-dispersive X-ray spectroscopy (EDS), and selected area electron diffraction (SAED) and were viewed as previously described (Langley and Beveridge, 1999). For samples analyzed by EDS, no stains were used on whole mounts and thin sections so that sorbed metal and mineral phases could be attributed only to the specific treatment. Whole-mount samples for TEM were prepared in the anaerobic chamber and were only exposed to air for ~30 s as they were moved from an airtight jar to the sample holder and inserted into the microscope. Embedded samples were likewise prepared under anaerobic conditions until the plastic polymerization step.

All imaging was performed with a Philips EM300 operating at 60 kV with a liquid nitrogen cold trap in place. SAED was performed on whole mounts of the culture, sampled at intervals, that were dropped onto carbon- and Formvar-coated Cu grids and held in an H_2/Ar atmosphere until being loaded into the microscope. Two electron microscopes were used for the diffraction: a Philips EM400T operating at 100 kV with a spot size of 50 nm, camera length of 574 mm, and an exposure time to record reflections of 20 s, and a LEO 912AB operating

Table 1. Final cell numbers, acetate/lactate ratio, and proportion of reduced Fe for CN32 cultured anaerobically for 46 d.

Electron acceptor	Cells (cfu/mL)	Acetate/lactate	Fe^{2+}/Total Fe
Fumarate	4×10^6	0.195	—
HFO	5×10^5	0.105	0.54 ± 0.09
Nano goethite	1×10^4	0.002	0
Micro goethite	5×10^2	0.001	0
Hematite	tftc[a]	0.002	0

[a] Too few to count.

at 100 kV with spot size 50 nm, camera length 580 nm, and 30-s exposure time.

EDS was similarly performed with two microscopes: first, the EM400T described above coupled to a Link Analytical LZ-5 X-ray detector, where spectra were collected over 100 s (live count time) with a beam diameter of ~400 nm at 100 kV and 25 mA beam current, and second, a Hitachi H7110 TEM operating in scanning transmission electron microscopy (STEM) nanoprobe mode and equipped with a Noran Voyager germanium detector. The spot size was 50 nm at 75 kV and a beam current of 25 mA.

2.7. XRD

For the mineral products formed during Fe reduction, XRD was performed on culture precipitates that were washed, dried, lightly crushed, and packed into Al-topfill holders in an H_2/Ar atmosphere, then scanned with a stream of O_2-free N_2 continuously flowing through the sample chamber. XRD scans were performed on a Rigaku Geigerflex horizontal goniometer under the following conditions: Co-Kα radiation, 45 kV, 25 mA, and 10 s per step with a step size of 0.02 °2θ, and divergence slit of 2°. Ground elemental Si was added to some samples as a standard. The Scherrer formula was used to calculate mean crystallite dimensions, or mean coherence lengths (MCLs) (Klug and Alexander, 1974).

3. RESULTS

3.1. Cell Growth and the Reduction of Goethite, Hematite, and HFO

Measurement of the redox potential showed that anaerobic conditions were reached 1 d after inoculation for all treatments. The pH remained close to the initial value of 6.5 for the treatments containing nanogoethite, microgoethite, and hematite, and increased gradually to 7.5 for HFO. The fumarate treatment initially fluctuated slightly in pH but became stable at pH 6.5 by 25 d. Concentrations of Fe^{2+} higher than the cell-free control were not found for the treatments containing hematite, nanocrystalline goethite, or microcrystalline goethite at any time during the 46-d experiment. Similarly, little acetate was produced, and cell numbers at termination were low (Table 1); acetate is an end product of anaerobic lactate metabolism for *S. putrefaciens* (Scott and Nealson, 1994). By contrast, 53% of total Fe had been reduced after 46 d in the samples with HFO, and the ratio of acetate/lactate showed that the cells had actively metabolized C. Final cell numbers (cfu/mL), although ~100-fold lower in the HFO treatment than at the time of inoculation, were significantly higher than was found for the crystalline Fe (hydr)oxides. As expected, growth was most vigorous when fumarate served as the electron acceptor, shown by the relatively high acetate/lactate ratio and final cell numbers (Table 1).
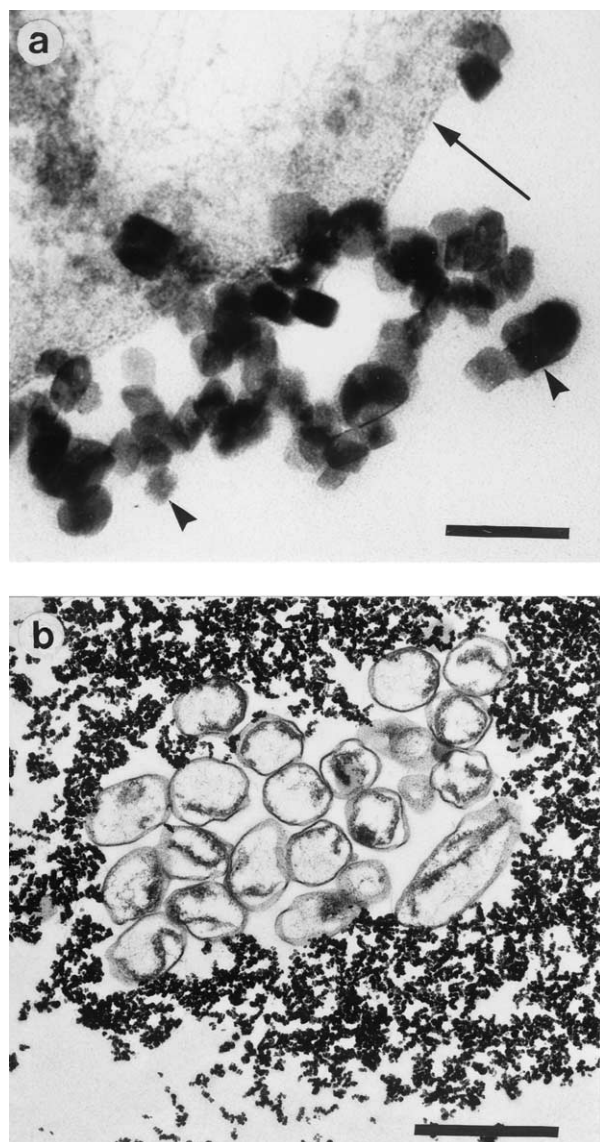
Fig. 1. Thin sections showing the association of *S. putrefaciens* CN32 cells with nanocrystalline Fe oxides after 1 week in anaerobic conditions. (a) Close-up of a cell showing hematite crystals attached to and penetrating the cell wall. Large arrow indicates cell wall, and arrowheads indicate hematite crystals. Scale bar = 250 nm. (b) CN32 cell cluster in a dilute suspension of goethite. The patchy appearance of the cells indicates that they are stressed or nonviable. Scale bar = 1 μm.

3.2. Association of Cells with Crystalline Minerals

We have found that minerals rapidly attach to cells cultured in air (Glasauer et al., 2001) as well as immediately after anaerobic conditions are established. Observations by TEM on whole mounts and sections of cells cultured anoxically with goethite and hematite minerals showed that a close association at the cell–mineral interface still existed after several days. It appeared that in some cases the minerals even penetrated the cell wall (Fig. 1). After 10 d, crystals were still found attached to the cells, although apparent structural changes indicated that many cells were stressed or no longer viable. The treatment
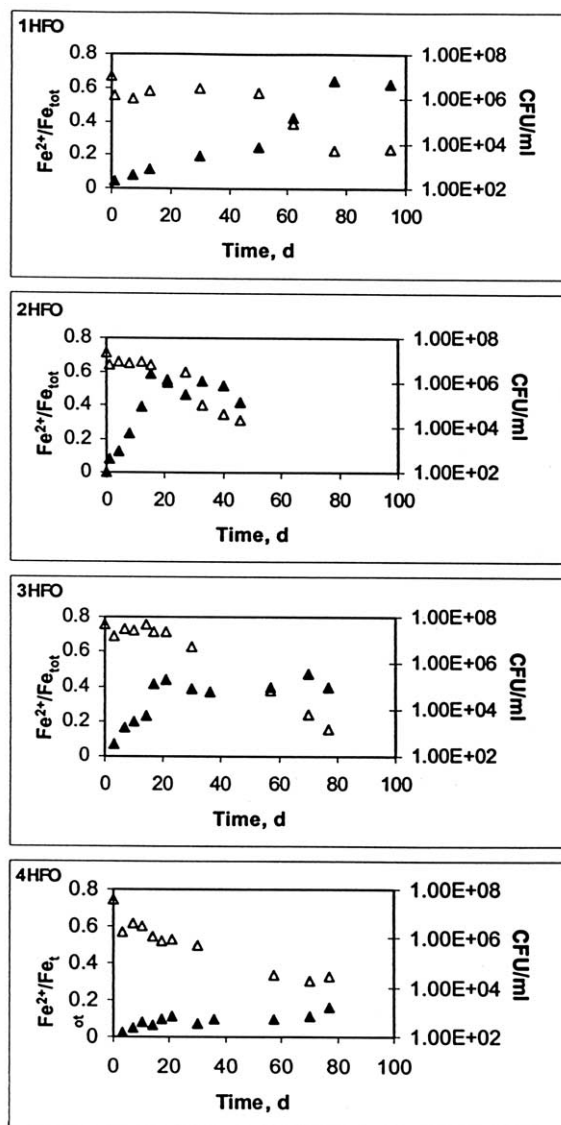
Fig. 2. Reduction of HFO, measured as Fe^{2+}/Fe_{tot} (solid triangles) and change in cell numbers (cfu/mL; open triangles) for anaerobic cultures of CN32 over time.

with nanogoethite exhibited an interesting phenomenon: tightly packed clusters of cells were surrounded by mineral crystals (Fig. 1). It is notable that these cultures had the highest survival rate among the treatments with the crystalline Fe minerals (Table 1). Cells in the HFO-grown cultures showed a similar tendency to aggregate. After 10 d, we were unable to find enough cells in the goethite or hematite cultures to make accurate observations. This was likely due both to die-off of the bacteria and to burial of the surviving or intact dead cells by the Fe minerals.

3.3. HFO Reduction and Mineral Formation

Additional reduction experiments were carried out with only HFO as the source of FeIII to follow the fate of reactive Fe more closely. We emphasize that biologic organisms are sen-
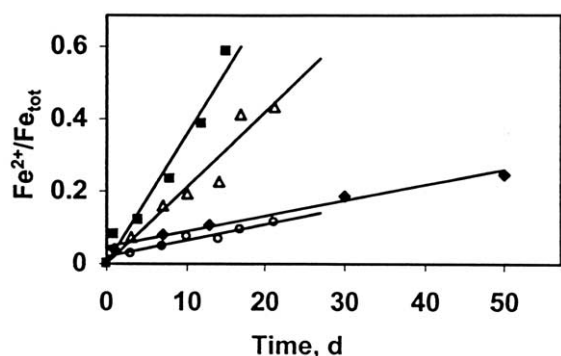
Fig. 3. Change in Fe^{2+} during initial dissolution of HFO by *S. putrefaciens* CN32. Data follow a linear equation. Filled diamonds show 1HFO, rate = 0.004 d^{-1}; filled squares show 2HFO, rate = 0.036 d^{-1}; open triangles show 3HFO, rate = 0.021 d^{-1}; open circles show 4HFO, rate = 0.005 d^{-1}.

sitive to small variations in their environment. Subtle differences in the inoculum size, the state of the cells in the inoculum, temperature, pH, etc., can all influence growth rate and cell numbers and could explain the variation in the rate of FeIII reduction that we observed. Such natural variability in reduction experiments with CN32 has been noted before (Fredrickson et al., 1998). Our results are, however, always consistent with respect to mineral formation.

3.3.1. Rate of Fe reduction

For 1HFO, the initial reduction rate was relatively slow (Fig 2). Reduction is expressed as the ratio Fe^{2+}/total Fe (Fe_t); this ratio is less variable than Fe^{2+} alone because rapid sedimentation of the newly forming precipitates made it difficult to collect samples that were representative of Fe^{2+} without also accounting for total Fe. The cfu/mL reached a plateau at 2×10^6, then gradually decreased over time. The experiment was terminated after 105 d, at which time the culture medium appeared brownish-black. At that point, Fe^{2+}/Fe_t was ~0.6.

The rates of Fe reduction for treatments 2HFO and 3HFO were comparable (Fig. 2). For 2HFO, the dark rust-brown growth medium became clear after 14 d, indicating complete transformation of the HFO, and a pale green precipitate formed. Fe^{2+} stabilized over the next 15 d, although cell numbers began to decrease gradually after Fe^{2+} peaked. A similar trend for Fe reduction was observed for 3HFO, but in this case, the precipitate that formed was a dark olive brown. Similar to 2HFO, cell numbers began to decline after Fe^{2+} reached the maximum value, although the cfu/mL decreased more slowly. Final Fe^{2+}/Fe_t was 0.5 for 2HFO and 0.4 for 3HFO. No P_i was detected in the culture medium when cell numbers began to decline. For all treatments, the pH increased from 6.5 to around 7.5 at termination, and the reduction potentials were around -320 mV.

Iron reduced slowly in 4HFO, the low P_i treatment (Fig. 2). Cell numbers were relatively low and constant throughout most of the experiment. This indicated that the culture reached a steady state at a lower population than in treatments where Fe reduction was more rapid. Reduced Fe remained low throughout the experiment; final Fe^{2+}/Fe_t was 0.1 at termination. The pH increased from 6.5 to 6.7 by the end of the experiment and

Table 2. Initial [P_i], initial rates of Fe reduction, and cell viability (CFU/mL) during respiration of CN32 on HFO.

Treatment	[P_i] (mM)	Initial rate of Fe reduction (d^{-1})	Day at CFU/mL = 10^{5a}
1HFO	4.0	0.0042 ($r^2 = 0.98$)	62
2HFO	4.0	0.0357 ($r^2 = 0.96$)	33
3HFO	4.0	0.0210 ($r^2 = 0.92$)	57
4HFO	0.4	0.0046 ($r^2 = 0.92$)	53

[a] Extrapolated from bracketing data points.

the final reduction potential was -140 mV. For the cell-free blank, less than 5% of Fe was reduced and 2-line ferrihydrite was the only mineral detected by XRD (data not shown).

Dissolution followed first-order kinetics during the initial weeks (Fig 3). Treatments 1HFO and 4HFO showed similarly low rates relative to 2HFO and 3HFO (Table 2). Treatments 2HFO and 3HFO were comparable, with 3HFO having a slightly lower rate. The time at which estimated cfu/mL had declined to 10^5 is inversely correlated with the rate of reduction for the treatments with higher P_i. Comparison of 4HFO with 1HFO reflects the poorer overall viability of the lower P_i treatment (Table 2).

3.3.2. Minerals

For treatments 1HFO, 2HFO, and 3HFO, the same variety of new minerals was observed from the time reduction began until the end of the experiment, although the proportions of minerals differed. We detected vivianite by 14 d, and powder XRD analyses of the precipitates on termination showed that vivianite predominated (Fig. 4). TEM of thin sections revealed that the vivianite had a divergent crystal habit, indicative of rapid crystallization, and formed in the matrix of HFO (Fig. 5a). TEM on whole-mount samples showed well-formed and highly crystalline particles up to 20 μm on an edge that were largely unassociated with cells. EDS confirmed that the minerals were rich in P and Fe (Fig 5b).

We also observed electron dense hexagonal crystals typical in size and shape for green rust (McGill et al., 1976; Mann et
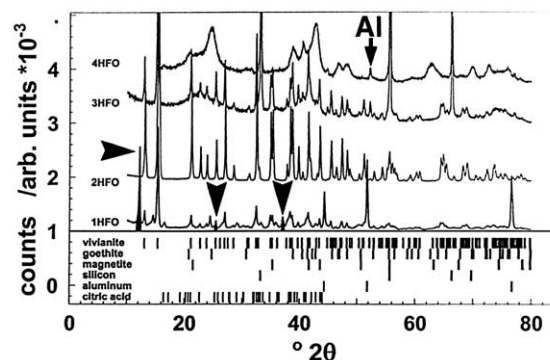

Fig. 4. XRD scans of precipitates formed during anaerobic Fe metabolism of HFO by *S. putrefaciens* CN32. Aluminum peaks originate from the sample holder; Si was added as internal standard to 3HFO and 4HFO. Unlabeled arrows to 1HFO peaks indicate green rust I.
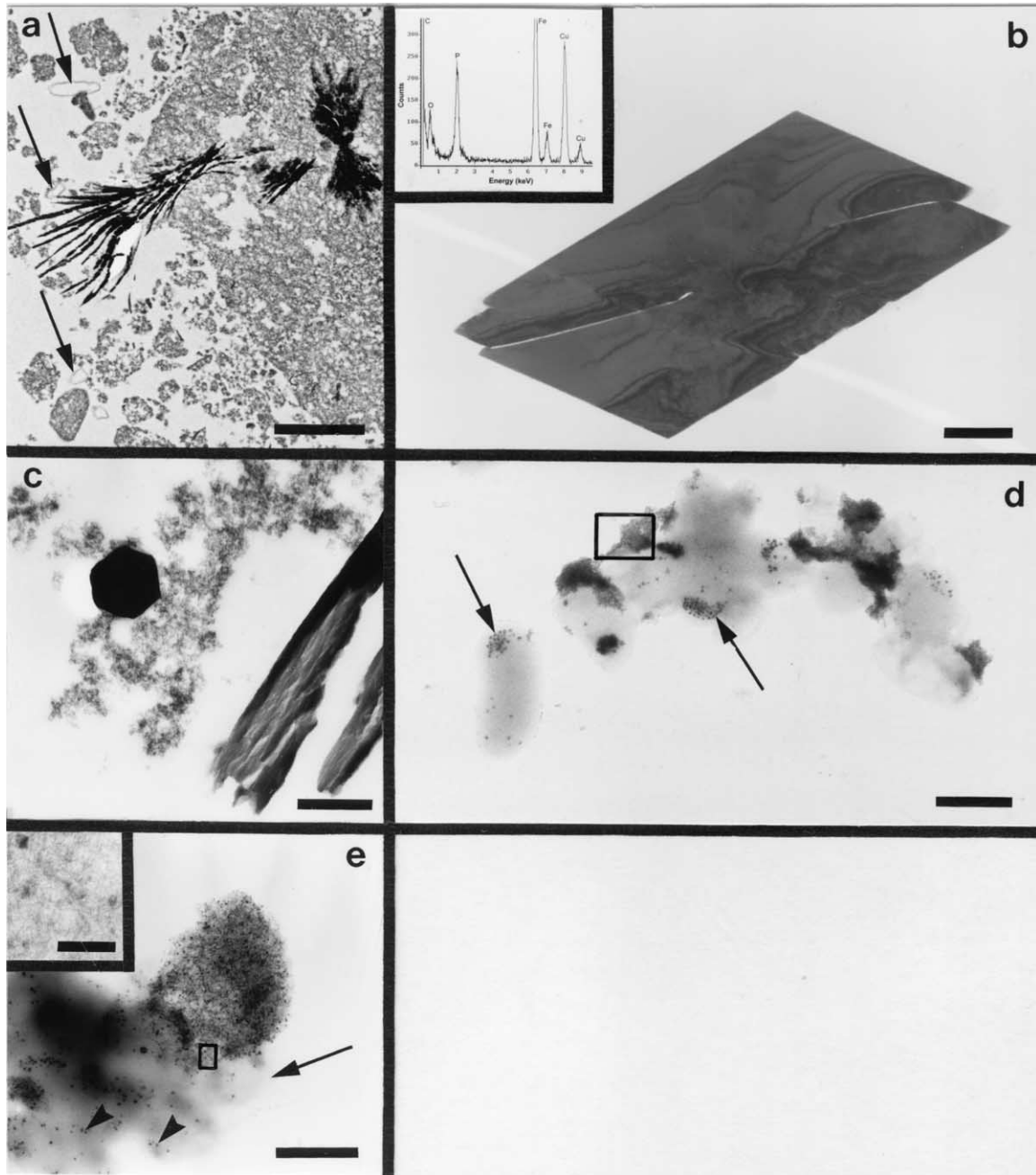
Fig. 5. Minerals formed during anaerobic Fe metabolism of HFO by *S. putrefaciens* CN32. (a) Thin section of 5-week suspension from 1HFO showing sheaflike bundles of vivianite forming in a matrix of HFO. Cells are indicated with an arrow. Scale bar = 3 μm. (b) Vivianite crystal observed in 4-week-old 2HFO. Scale bar = 10 μm. EDS inset indicates high amounts of Fe and P. (c) Thin section showing hexagonal crystal of green rust associated with HFO, observed in 3-week suspension from 3HFO. Dark bands to the right of the image are vivianite crystals. Scale bar = 250 nm. (d) Cluster of CN32 cells associated with transforming HFO, observed in 2-week suspension from 1HFO. Circled area contains tiny dark particles of magnetite in an HFO aggregate. Arrows indicate intracellular granules. Scale bar = 1 μm. (e) Cluster of CN32 cells associated with transforming HFO observed in 2-week suspension from 3HFO. Inset reveals that the aggregate consists of tiny needlelike particles and magnetite. Arrows indicate cells and arrowheads show intracellular granules. Scale bar = 1 μm; inset, bar = 100 nm.

al., 1989; Fredrickson et al., 1998). Green rusts are Fe(II)-Fe(III) layered double hydroxysalts found in hydromorphic sediments and are precursors to magnetite, vivianite, goethite, and lepidocrocite (Mann et al., 1989; Hansen and Poulsen, 1999; Benali et al., 2001; Génin et al., 2001). They have the general formula $[\text{Fe}^{II}_{(1-x)}\text{Fe}^{III}_{x}(\text{OH})_{2}]^{x+} \cdot [(x/n)\text{A}n\text{-} \cdot (m/n)\text{H}_2\text{O}]^{x-}$, where x is the ratio $\text{FeIII}/\text{Fe}_{tot}$ and reflects the structure of brucitelike layers with interlayer anions An- and

water molecules (Génin et al., 2001). Chloride and OH^- (GRI) and SO_4^{2-} and CO_3^{2-} (GRII) are typical interlayer ions. EDS on representative green rust crystals showed high amounts of Fe with traces of Cl and P. The crystals were observed throughout the early to mid time range of sampling, but the mineral was detected by powder XRD only for 1HFO (Fig. 4). By the end of the experiment, the green rust that formed in 2HFO and 3HFO had either converted to vivianite or was below the detection limits of XRD and TEM observations. In the case of 1HFO, the XRD peaks at 12.15, 25.42, and 37.05°2θ indicated green rust I, with a layer thickness of 0.85 nm (Génin et al., 2001). The full width at half maximum height (FWHM) of the 001, 002, and 003 reflection series was used to calculate an average crystal thickness of 250 nm. We observed an average crystal diameter of 2 to 3 μm, which yields an aspect ratio (diameter to thickness) that is within the range reported for green rust (Scherer et al., 1999). As observed for vivianite, the green rust crystals appeared to form mainly away from the bacteria and were often associated with HFO (Fig. 5c). Similar observations on the spatial separation of cells and vivianite or green rust have been made in previous studies (Jorand et al., 2000; Parmar et al., 2001).

Magnetite crystallites were < 10 nm in diameter and were located within aggregates of HFO associated with cells (Fig. 5d). Electron diffraction patterns were typical for small or poorly crystalline biogenic magnetite (Fredrickson et al., 1998). Aggregates of tiny (5 to 10 nm long) crystals with a needlelike crystal habit, suggestive of goethite, were sometimes associated with magnetite in the HFO matrix (Fig. 5e). Electron diffraction on isolated patches of the crystallites showed patterns consistent with HFO, although with indications of more structural order. The difficulty we experienced in obtaining distinct electron diffraction patterns in these samples is most likely owing to the poor crystal order and small size of the crystallites. For the same reason, goethite could not be accurately detected by XRD; any XRD lines would be broad, of low intensity, and masked by other peaks. Magnetite was, however, detected by XRD in 1HFO, which confirmed that the mineral was poorly ordered and present in small quantities. 3HFO also contained poorly crystalline ferric oxide, as indicated by a broad background peak at around 40°2θ (Fig. 4).

For 4HFO, it was very difficult after 1 week to identify cells among the abundant, electron-dense, and Fe-rich material. TEM observations on thin sections revealed cells encrusted with a fine-grained Fe phase similar to the tiny elongated crystallites we observed for the other HFO treatments (Fig. 6). Goethite was the only mineral phase detected by XRD (Fig. 4). EDS and electron diffraction analyses showed poorly crystalline Fe-rich material, although reflections indicative for goethite were also seen (Fig. 6). At the end of the experiment, the medium had a dark olive-brown color similar to 1HFO and 3HFO. A replicate treatment confirmed the results.

To observe the influence of cell population size on the rate of Fe reduction and mineral transformation, an additional treatment identical to 1, 2, and 3 except for a higher inoculum of cells (10^9 cfu/mL) was carried out. In this case, HFO transformed completely to a pale green precipitate by 7 d and vivianite was the only mineral detected by XRD.

3.3.3. Intracellular minerals

For treatments 1, 2, and 3, we observed microscopic intracellular grains of a nonmagnetic amorphous Fe oxide material, as reported elsewhere (Glasauer et al., 2002). Grains appeared in the cells, concentrated at the cell poles, after Fe reduction began and increased in number over time (Figs. 5d,e). Cells containing them appeared particularly healthy, which we determined by the large size of the cells, the homogeneity of the cytoplasm, and the existence of intact membranes. Dead cells, judged by the mottled appearance of the cytoplasm and discontinuity of the cell wall, did not contain the intracellular particles. For 4HFO, the copious amount of mineral phase that attached to the cells made it impossible to view any internal details of the bacteria, and no signs of the grains were seen in TEM thin sections.

4. DISCUSSION

4.1. Respiration with HFO, Goethite, and Hematite

Growth conditions in natural environments are usually more constrained by nutritional limitations than are those found in most laboratory growth media, yet subsurface bacteria should be able to manufacture most of what they need from a simple medium that does not include complex growth factors (Ingraham et al., 1983). One consequence of growth in an enriched medium for *S. putrefaciens* is the increased production of metal-reducing proteins known as cytochromes (Obuekwe and Westlake, 1982). Membrane-bound cytochromes play a key role in Fe reduction by *S. putrefaciens* (Myers and Myers, 1992; DiChristina et al., 2002), and the influence of different culture media on their production demonstrates how profoundly sensitive bacteria are to the growth conditions. This is not surprising because prokaryotes have great metabolic plasticity. It is likely that many factors involved in reduction will be affected as the cell adjusts to the environment (Koch, 1985). Our results demonstrate how conditions that are more nutritionally limited than those previously used for metal reduction experiments with CN32 (e.g., Fredrickson et al., 1998; Zachara et al., 1998) restrict the Fe mineral that can be used for anaerobic growth. At the same time, the rate of Fe reduction under these more stringent conditions determined the mineral products that resulted when FeIII reduction did occur, as discussed below.

Cells associate with preformed minerals by attachment at the cell wall or via capsules and extracellular polysaccharides (Beveridge, 1989; Glasauer et al., 2001). Although cell–mineral contact facilitates reduction, contact with an FeIII mineral is not sufficient for reduction to take place. This is demonstrated in particular by our attempt to reduce nanogoethite, a mineral of relatively poor crystallinity and large specific surface area (Glasauer et al., 1999), with CN32. Reduction potentials of goethite and hematite are below −200 mV on the basis of crystal size and structure, with hematite being slightly lower, whereas this value is much higher for HFO (Table 3). Given the values of the reduction potentials that we measured for the goethite and hematite treatments (>−110 mV), it is expected that the crystalline minerals will not be reduced. By contrast, measured reduction potentials were significantly lower for the HFO treatments (<−300 mV). During respiration, bacteria
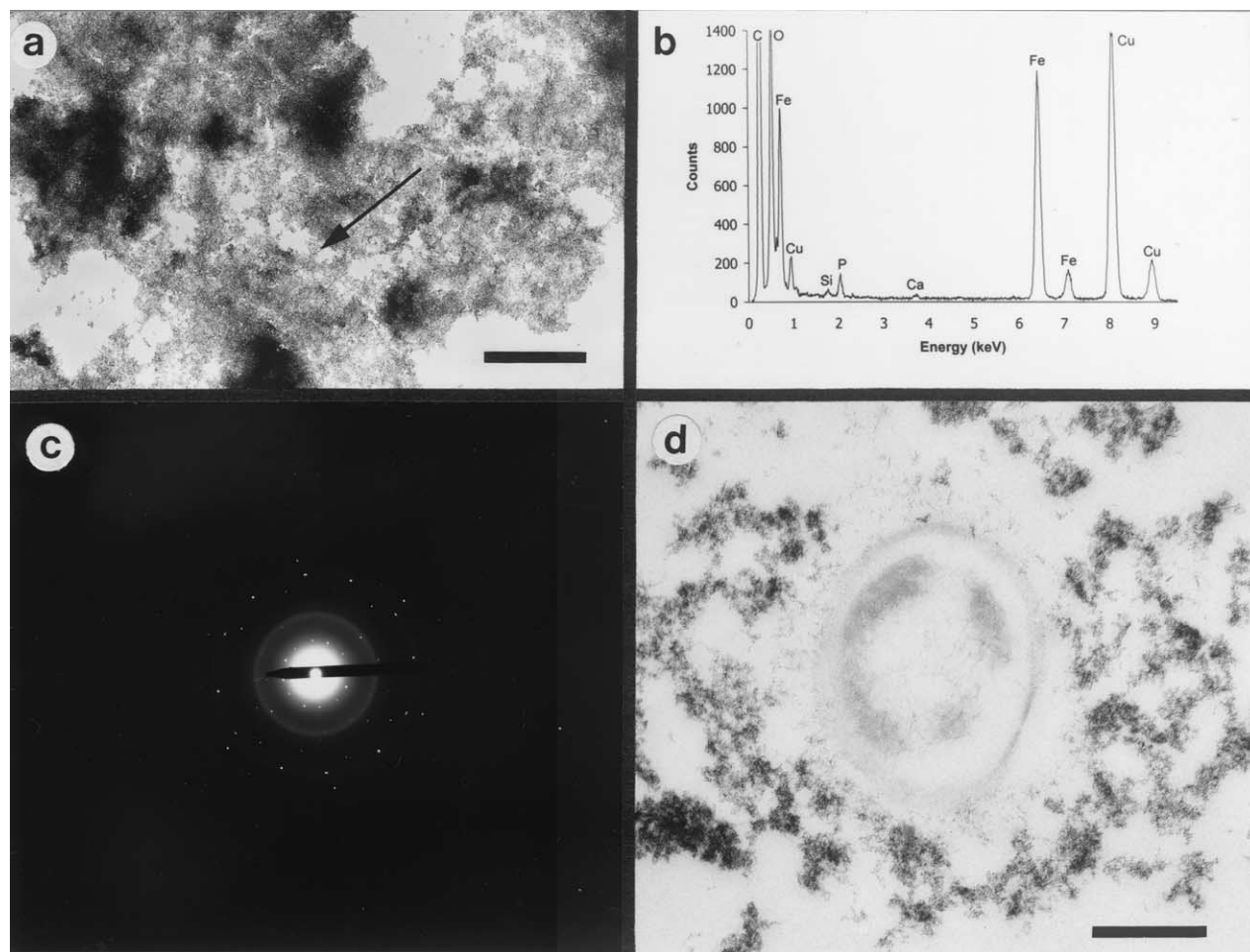
Fig. 6. Transformation of HFO during anaerobic metabolism of *S. putrefaciens* CN32 with low PO_4^{3-} (4HFO). (a) Fine-grained electron-dense material observed in suspension from 4HFO after 7 weeks. Scale bar = 500 nm. (b) EDS and (c) electron diffraction patterns of material shown in (a) indicating that the phase is rich in Fe and O, contains traces of P and goethite, and is microcrystalline. Cu peaks in the EDS spectrum originate from the EM grid. (d) Thin section of pellet from 3-week 4HFO suspension showing cell surrounded by fine-grained mineral phase outside a layer of extracellular polysaccharide. Nascent crystallites of goethite can be seen in the HFO matrix. Scale bar = 250 nm.

lower the overall reduction potential by using available electron acceptors having half-reactions of increasingly negative potential, in accordance with soluble species found along redox gradients. Reducing conditions are established once O_2 is consumed, followed by reduction of, for example, MnIV, NO_3^-, FeIII, organic, and SO_2^- species (Stumm and Morgan, 1996). It is probable that in studies with DIRB that show reduction of crystalline Fe minerals the use of higher inocula and more rapidly metabolizing cells established more favorable redox conditions. Furthermore, this raises the possibility that crystal-

line FeIII minerals might be more readily reduced by *Shewanella* if HFO is also present.

Other factors also likely contribute to the reductive dissolution of minerals mediated by bacteria—that is, the expression of reductases or other factors produced by the cell, and the surface structure and solubility of the mineral. Fe(hydr)oxide solubilities are relatively low among metal oxides and generally follow the trend: HFO > goethite > hematite, with values of the solubility products around $10^{-38.8}$, $10^{-41.5}$, and $10^{-42.7}$, respectively (Smith and Martell, 1976).

Table 3. Reduction potentials of HFO ($Fe(OH)_3$), goethite (FeOOH) and hematite (Fe_2O_3).[a]

Half-reaction	E_o (V)	E' (V)	Source
$Fe(OH)_{3(s)} + 3H^+ + e^- = Fe^{2+} + 3H_2O$	+1.06	+0.17	Lindsay (1979)
$FeOOH_{(s)} + 3H^+ + e^- = Fe^{2+} + 2H_2O$	+0.67	−0.22	Stone and Ulrich (1989)
$1/2Fe_2O_{3(s)} + 3H^+ + e^- = Fe^{2+} + 3/2H_2O$	+0.66	−0.23	Stone and Ulrich (1989)

[a] E_o = standard reduction potential; E' = reduction potential with $[H^+] = 1.0 \times 10^{-7}$ mol/L, [Fe] = 1.0×10^{-6} mol/L.

Although cells did not use the crystalline Fe minerals we supplied as the terminal electron acceptor, they survived for several weeks (in the case of hematite) or for the length of the experiment (in the case of nano- and microgoethite) under anaerobic conditions. They may have used organic metabolites from lysed cells for electron acceptors and existed as aggregates in a state of cell–cell cooperation to increase survival, such as the cell clusters we observed (Dawes, 1985; Lewis and Gattie, 1990).

4.2. Mineral Formation

4.2.1. Sensitivity to culture conditions

In making observations on the relationship between cells and minerals, there was a balance to achieve between sampling for observing the minerals vs. sampling for observing the cells. The former naturally existed in the greatest variety and amount at the point in time when cell numbers were dropping and the bacteria were difficult to find. From our observations, it is, however, apparent that vivianite and green rust did not nucleate on the cell surface. Neither did fine-grained magnetite and goethite form on the cells, but rather in the matrix of cell-associated HFO. Hydrous ferric oxide and Fe^{2+} transform readily to magnetite via green rust (Mann et al., 1989); if sufficient Fe^{2+} and P_i are available, vivianite may form (Emerson and Widmer, 1978; Fredrickson et al., 1998). The location of the HFO and the local concentrations of the necessary ionic species determine where the minerals crystallize.

As explained in the "Results," treatments 1HFO, 2HFO, and 3HFO differed in the final proportions of minerals that had formed once cell activity essentially ceased, rather than in the kinds of minerals. In batch culture, it is difficult to produce an identical cell population even under apparently identical conditions. The experimental conditions may have established the cell population near an equilibrium point, where slightly more favorable conditions tipped the balance toward a faster rate of Fe reduction and the consequent formation of a higher proportion of vivianite. In natural environments, cells are subject to wide variations in conditions as a result of seasonal variations that affect nutrient supply, hydration, pH, and Eh, which in turn affects mineral formation. For example, the formation of gypsum and calcite by *Synechococcus* GL24 exhibits strong seasonal dependence in Fayetteville Green Lake, New York, USA (Douglas and Beveridge, 1998).

4.2.2. Mineral formation as a function of microenvironments

The minerals that we observed are consistent with the low reduction potentials created by the respiring bacteria and are observed in a range of subsurface environments. Mineral stability calculations predict that under our experimental conditions vivianite and magnetite will coexist (Stumm and Morgan, 1996; Fredrickson et al., 1998), which we observed. However, such calculations do not capture the microheterogeneity of cell-influenced environments.

Magnetite is a common product of dissimilatory Fe reduction by bacteria (Bazylinski and Moskowitz, 1997). It has an inverse spinel structure and contains 1/3 FeII in octahedral sites and 2/3 FeIII divided between octahedral and tetrahedral sites. In the HFO treatments, the immediate cell environment sustained the

conditions for magnetite crystallization by providing Fe^{2+}, which produces Fe^{3+} via the reductive dissolution of ferrihydrite; this is one known pathway for the formation of magnetite (Cornell and Schwertmann, 1996). The Fe^{2+}-catalyzed reduction of Fe oxides is accelerated by Cl^- and by complex-forming molecules in a reducing environment (Segal and Sellers, 1980; Arnold et al., 1986a; Cornell and Schwertmann, 1996); in the present study Cl^- was abundant in the culture medium and Fe-complexing organic acids are common constituents of bacterial cells. A second likely pathway for magnetite formation is via green rust. The cooccurrence of magnetite and goethite has been observed in abiotic systems during formation in HFO-FeII systems via a green rust intermediate (Mann et al., 1989), and our study similarly shows that both minerals crystallized in the cell-influenced environment at the expense of HFO. Because P_i slows the rate of green rust transformation to magnetite (Mann et al., 1989), the immediate extracellular environment was likely depleted in P_i because of cell uptake and hence favored magnetite over vivianite.

The green rust phase we observed is consistent with Cl^--GR. The higher layer thickness of 0.85 nm, as compared with pure Cl^--GR with a value of 0.80 nm (Refait and Génin, 1993), suggests that some PO_4^{3-}, or CO_3^{2-} produced during C metabolism may have entered the interlayer, thus widening it to 0.85 nm (Hansen and Poulsen, 1999). The crystallization of green rust is inhibited by P_i, and P_i destabilizes green rust in favor of vivianite (Hansen and Poulsen, 1999; Benali et al., 2001); hence, the formation of vivianite precipitated P_i from solution and likely facilitated the formation and eventual transformation of the green rust. The observation that green rust was occasionally seen at the cell surface as well as away from cells reflects its role as a precursor to both magnetite and vivianite.

Vivianite was ubiquitous in the treatments with 4 mM P_i. The formation of vivianite away from the cells and within the HFO aggregates reflects variations in P_i. As explained for the formation of magnetite, Fe^{2+} diffusing into an HFO aggregate can catalyze the reductive dissolution of FeIII; the concentration of P_i further from the cells probably favored vivianite formation. In terms of net mineral growth, our results show that fast biotic Fe reduction selects for the crystallization of vivianite, in agreement with the results of others (Jorand et al., 2000; Fredrickson et al., 1998). However, we also observed that the rate of formation, the relative quantity formed and the crystallinity are influenced by the rate of Fe reduction. Although the absolute concentration of P_i was identical for treatments 1, 2, and 3, 2HFO, and 3HFO had more Fe(II) per unit time in solution, as inferred from their faster rate of Fe reduction. The concentration of P_i in these systems should favor vivianite over green rust (Fredrickson et al., 1998), which we observed. However, for 1HFO we detected larger amounts of green rust and magnetite. Because vivianite is the predicted stable phase, this indicates that green rust crystallized before vivianite, and then partially transformed. Furthermore, at the pH of 6.5 to 7.0 in our system, HFO should transform to green rust if Fe^{2+} is present (Hansen and Poulsen, 1999). Hence, the faster FeII is released, the faster green rust forms, but then readily transforms into vivianite if sufficient FeII and P_i are available. The MCLs calculated after Scherrer (Klug and Alexander, 1974) for the vivianite have values of 246, 287, and 530 nm for 1HFO, 2HFO and 3HFO, respectively. This corre-

lates with the initial rate of FeII production (Table 2) and indicates higher vivanite stability where FeII production is higher.

The highest measured values of Fe^{2+} were ~50 to 65% of total Fe, or 4 to 5 mM. The ratio of FeII/P in vivianite is 3:2; because total P_i in the culture flasks was 4 mM, 66 to 83% of the P was structural in the vivianite when the experiments were completed. The remaining P_i may have been incorporated into other minerals or sorbed, and was bound into the biomass of the few remaining cells and organic compounds released when the cells lysed. The formation of vivanite effectively outcompeted cells for available P_i.

In the case of 4HFO, the low $[P_i]$ and the slow rate of Fe^{2+} production were linked through the influence of P on cell fitness. Sufficient Fe^{2+} was produced by the slowly metabolizing cells to catalyze the reductive dissolution of HFO (Cornell and Schwertmann, 1996), which supplied Fe^{3+} for the crystallization of goethite. Goethite is believed to form by dissolution of a ferrihydrite precursor and subsequent nucleation rather than by structural rearrangement (Cornell and Schwertmann, 1996). The relatively low MCL of 9 nm calculated for the goethite indicates that the mineral was poorly crystalline, in agreement with TEM observations. Although the cells were largely coated with sorbed minerals, cell counts prove that they were viable until termination of the experiment. It may be that cells associated closely with the extracellular minerals to gain P for growth, which would be liberated by reduction of FeIII. FeIII(hydr)oxide saturated with P_i is readily reduced by DIRB (Lovley and Phillips, 1986b).

4.2.3. Relevance to natural environments

Vivianite is diagnostic for low redox potential (Eh ~ -0.2 to -0.4 V) and is likely the most stable FeII orthophosphate solid phase in some anaerobic sedimentary environments (Nriagu, 1972; Emerson, 1976). Studies of diagenesis in anaerobic sediments have found vivianite in equilibrium with interstitial pore waters (Bray et al., 1973; Emerson and Widmer, 1978), and there is strong evidence that vivanite formation in natural subsurface environments can be mediated by microorganisms (Mucci et al., 2000; Stamatakis and Koukouzas, 2001). Emerson (1976) attributed the existence of vivianite in anaerobic lake sediments to the outcome of rate-controlled processes, in particular to the rate of organic matter degradation, for which the flux of phosphate was probably responsible. Under conditions of low P_i, we observed that mineral formation shifted from vivianite to goethite, which can be explained by insufficient Fe^{2+} and P_i for vivianite, and insufficient Fe^{2+} for magnetite formation, as well as by P-limited cell growth. It is likely that, in treatments where faster Fe reduction and subsequent vivianite formation took place, consumption of P_i by the forming vivianite impacted cell growth and led to decline of the cell population. In support of this, no P_i was detected when cell numbers began to decline, whereas C was still abundant; cell survival was higher when vivianite formed more slowly. Phosphate is an essential component of cell membranes, proteins and ribonucleic acids necessary for maintenance and growth of cells.

Mineral formation and P_i uptake by organisms are competitive processes, particularly if the minerals contain significant structural P. Although bacterially mediated reduction of poorly crystalline Fe can release P_i (Jansson, 1987; Gächter et al., 1988), the subsequent formation of new minerals can remove P_i from the labile pool (Emerson and Widmer, 1978). Relatively high concentrations of Fe^{2+} are necessary to stabilize vivianite, however, and the Fe and P_i immobilized in vivianite are readily available (Nriagu, 1972). It has been hypothesized that at the time when the first life forms developed, the aqueous environment was richer in soluble phosphate than at the present time, and P_i probably fell within the vivianite stability field (Gulick, 1955; Nriagu, 1972). The formation of P-rich sedimentary minerals that are observed today has been attributed to the activities of early cellular life (Gedulin and Arrhenius, 1994). Given the strong possibility that primitive prokaryotes utilized the FeII/FeIII couple for respiration (Vargas et al., 1998), vivianite may have been much more widespread than it is today.

The formation of goethite under the condition of relatively low P_i is relevant to a wide range of modern subsurface and aquatic environments because phosphate is often a limiting nutrient (Schindler, 1977; Hudson et al., 2000; Wu et al., 2000). In a CO_3^{2-}-free environment, the outcome of abiotic ferrihydrite transformation in a reducing environment is lepidocrocite (Carlson and Schwertmann, 1990) or nano-sized goethite (Weidler, unpublished data), but neither of these minerals was observed in the cell-free control. Some CO_3^{2-} may have accumulated from cell metabolic processes. As was observed for the treatments with 4 mM P_i, reduction of Fe by CN32 likely catalyzed a process that occurs more slowly under abiotic conditions.

In natural environments where microorganisms are active, mineral formation will be affected by cellular microenvironments—that is, the immediate local environment found close to a cell or group of cells. Then, as minerals form, these phases also alter the cellular microenvironment so that a constant interplay between cell and mineral formation must continuously occur. In our experiments, the treatment with low P_i demonstrates that CN32 influences mineral formation even under nutrient-limited conditions and at low cell densities. The superposition of equilibria that results in such heterogeneous systems can lead to complex assemblages of minerals, such as we observed during reduction of HFO by CN32. It has been shown that biotic and abiotic processes of mineral formation are interdependent and, in some cases, inseparable (Sørensen and Jørgensen, 1987; Nealson et al., 1989; Canfield et al., 1993). Strictly abiotic studies on the dynamics of metal reduction and mineral formation under reducing conditions may translate poorly to many natural environments because of the intricate link between inorganic processes and the microorganisms providing the raw materials that fuel the reactions (e.g., Myeni et al., 1997; Génin et al., 2001). To understand how extensive the influence of bacteria can be, it is essential to assess which minerals are available for reduction by bacteria growing under typical conditions. We recognize that our experimental design is still far from modeling most natural environments and this work represents our initial efforts at approaching conditions in the environments where these bacteria are found.

5. CONCLUSIONS

The attachment of DIRB to minerals containing FeIII under reducing conditions is not evidence that the bacteria are reducing Fe. *S. putrefaciens* CN32 is typically cultured in nutrient-rich broth; however, when grown under nutrient-limited conditions more typical of the subsurface environments where the bacterium is found, only poorly crystalline hydrous ferric oxide was reduced. Cells were found to strongly attach to the FeIII minerals we examined, indicating possible recognition of the metal species or favorable electrostatic interactions even when the energetics for reduction were unfavorable. The variety of minerals that formed when reduction of HFO occurred highlights the interplay between the rate of Fe^{2+} production and cell-mediated microenvironments. Along the pathway to formation of vivianite, which was the stable end product when P_i was not initially limiting, we observed green rust, magnetite, and goethite. Pure goethite resulted when the HFO surface was undersaturated with respect to P. These results support a key role for P_i and hydrous ferric oxide phases for mineral formation in anaerobic sedimentary environments.

REFERENCES

Arnold R. G., DiChristina T. J., and Hoffman M. R. (1986a) Reductive dissolution of Fe(III) oxides by *Pseudomonas* sp. *200. Biotechnol. Bioeng.* **32,** 1081–1096.

Arnold R. G., DiChristina T. J., and Hoffman M. R. (1986b) Inhibitor studies of dissimilative Fe(III) reduction by *Pseudomonas* sp. strain *200* ("*Pseudomonas ferrireductans*"). *Appl. Environ. Microbiol.* **52,** 281–289.

Bazylinski D. A. and Moskowitz B. M. (1997) Microbial biomineralization of magnetic iron minerals: Microbiology, magnetism and environmental significance. In *Geomicrobiology: Interactions between Microbes and Minerals* (eds. J. F. Banfield and K. H. Nealson), pp. 181–223. Reviews in Mineralogy Vol. 35. Mineralogical Society of America.

Benali O., Abdelmoula M., Refait P., and Génin J. M. R. (2001) Effect of orthophosphate on the oxidation products of Fe(II)-Fe(III) hydroxycarbonate: The transformation of green rust to ferrihydrite. *Geochim. Cosmochim. Acta* **65,** 1715–1726.

Beveridge T. J. (1981) Ultrastructure, chemistry and function of the bacterial wall. *Int. Rev. Cytol.* **72,** 229–317.

Beveridge T. J. (1989) Metal ions and bacteria. In *Metal Ions in Bacteria* (eds. T. J. Beveridge and R. J. Doyle), pp. 1–30. Wiley.

Bray J. T., Bricker O. P., and Troup B. N. (1973) Phosphate in interstitial waters of anoxic sediments: Oxidation effects during sampling procedures. *Science* **180,** 1362–1363.

Burdige D. J. and Nealson K. H. (1986) Chemical and microbiological studies of sulfide mediated manganese reduction. *Geomicrobiol. J.* **4,** 361–87.

Canfield D. E., Thamdrup B., and Hansen J. W. (1993) The anaerobic degradation of organic matter in Danish coastal sediments: Iron reduction, manganese reduction, and sulfate reduction. *Geochim. Cosmochim. Acta* **57,** 3867–3883.

Carlson L. and Schwertmann U. (1990) The effect of CO_2 and oxidation rate on the formation of goethite versus lepidocrocite from an Fe(II) system at pH 6 and 7. *Clay Minerals* **25,** 65–71.

Clarke A. J. (1993) Extent of peptidoglycan O acetylation in the tribe *Proteeae. J. Bacteriol.* **175,** 4550–4553.

Collins Y. E. and Stotzky G. (1992) Heavy metals alter the electrokinetic properties of bacteria, yeasts and clay minerals. *Appl. Environ. Microbiol.* **58,** 1592–1600.

Cornell R. M. and Schwertmann U. (1979) Influence of organic anions on the crystallization of ferrihydrite. *Clays Clay Minerals* **27,** 402–410.

Cornell R. M. and Schwertmann U. (1996) *The Iron Oxides: Structure, Properties, Reactions, Occurrence and Uses.* VCH Verlag.

Daughney C. J. and Fein J. B. (1998) The effect of ionic strength on the adsorption of H^+, Cd^{2+}, Pb^{2+} and Cu^{2+} by *Bacillus subtilis* and *Bacillus licheniformis*: A surface complexation model. *J. Coll. Int. Sci.* **198,** 53–77.

Dawes E. A. (1985) Starvation, survival and energy reserves. In *Bacteria in Their Natural Environments* (eds. M. Fletcher and G. D. Floodgate), pp. 43–80. Special publication of the Society for General Microbiology 16. Academic Press.

DiChristina T. J., Moore C. M., and Haller C. A. (2002) Dissimilatory Fe(III) and Mn(IV) reduction by. *Shewanella putrefaciens* requires ferE, a homolog of the pulE (gspE) type II protein secretion gene. *J. Bacteriol.* **184,** 142–151.

Douglas S. and Beveridge T. J. (1998) Mineral formation by bacteria in natural microbial communities. *FEMS Microbiol. Ecol.* **26,** 79–88.

Emerson S. (1976) Early diagenesis in anaerobic lake sediments: Chemical equilibria in interstitial waters. *Geochim. Cosmochim. Acta* **40,** 925–934.

Emerson S. and Widmer G. (1978) Early diagenesis in anaerobic lake sediments—II. Thermodynamic and kinetic factors controlling the formation of iron phosphate. *Geochim. Cosmochim. Acta* **42,** 1307–1316.

Fein J. B., Daughney C. J., Yee N., and Davis T. A. (1997) A chemical equilibrium model for metal adsorption onto bacterial surfaces. *Geochim. Cosmochim. Acta* **61,** 3319–3328.

Ferris F. G., Beveridge T. J., and Fyfe W. S. (1986) Iron–silica crystallite nucleation by bacteria in a geothermal sediment. *Nature* **320,** 609–611.

Ferris F. G., Fyfe W. S., and Beveridge T. J. (1987) Bacteria as nucleation sites for authigenic minerals in a metal-contaminated lake sediment. *Chem. Geol.* **63,** 225–232.

Fortin D., Ferris F. G., and Scott S. D. (1998) Formation of Fe-silicates and Fe-oxides on bacterial surfaces in samples collected near hydrothermal vents on the Southern Explorer Ridge in the northeast Pacific Ocean. *Am. Mineral.* **81,** 1399–1408.

Fredrickson J. K., Zachara J. M., Kennedy D. W., Dong H., Onstott T. C., Hinman N. W., and Li S. (1998) Biogenic iron mineralization accompanying the dissimilatory reduction of hydrous ferric oxide by a groundwater bacterium. *Geochim. Cosmochim. Acta* **62,** 3239–3257.

Gächter R., Meyer J. S., and Mares A. (1988) Contribution of bacteria to release and fixation of phosphorus in lake sediments. *Limnol. Oceanogr.* **33,** 1542–1558.

Gedulin B. and Arrhenius G. (1994) Sources and geochemical evolution of RNA precursor molecules: The role of phosphate. In *Early Life on Earth* (ed. Stefan Bengtson), Nobel Symposium 84. Columbia University Press, New York.

Génin J.-M. R., Refait P., Bourrié G., Abdelmoula M., and Trolard F. (2001) Structure and stability of the Fe(II)-Fe(III) green rust "fougerite" mineral and its potential for reducing pollutants in soil solutions. *Appl. Geochem.* **16,** 559–570.

Glasauer S., Friedl J., and Schwertmann U. (1999) Properties of goethites prepared under acidic and basic conditions in the presence of silicate. *J. Colloid. Interface Sci.* **216,** 106–115.

Glasauer S., Langley S., and Beveridge T. J. (2001) Sorption of Fe(hydr)oxides to the surface of. Shewanella putrefaciens: Cell-bound fine-grained minerals are not always formed de novo. *Appl. Environ. Microbiol.* **67,** 5544–5550.

Glasauer S., Langley S., and Beveridge T. J. (2002) Intracellular iron minerals in a dissimilatory iron-reducing bacterium. *Science* **295,** 117–119.

Gulick A. (1955) Phosphorus as a factor in the origin of life. *Am. Sci.* **43,** 479–489.

Hansen H. C. B. and Poulsen I. G. (1999) Interaction of synthetic sulphate "green rust" with phosphate and the crystallization of vivianite. *Clays Clay Minerals* **47,** 312–318.

Hudson J. J., Taylor W. D., and Schindler D. W. (2000) Phosphate concentrations in lakes. *Nature* **406,** 54–56.

Ingraham J. L., Maaløe O., and Neidhardt F. C. (1983) *Growth of the Bacterial Cell.* Sinauer.

Jansson M. (1987) Anaerobic dissolution of iron–phosphorus complexes in sediment due to the activity of nitrate-reducing bacteria. *Microb. Ecol.* **14,** 81–89.

Jorand F., Appenzeller B. M. R., Abdelmoula M., Refait P., Block J.-C., and Génin J.-M. R. (2000) Assessment of vivianite formation in *Shewanella putrefaciens* culture. *Environ. Technol.* **21,** 1001–1005.

Klug H. P. and Alexander L. E. (1974) *X-Ray Diffraction Procedures for Polycrystalline and Amorphous Materials.* 2nd ed. Wiley.

Koch L. (1985) The macroeconomics of bacterial growth. In *Bacteria in Their Natural Environments* (eds. M. Fletcher and G. D. Floodgate), pp. 1–42. Special publication of the Society for General Microbiology 16. Academic Press.

Kostka J. E., Haefele E., Vieweger R., and Stucki J. W. (1999) Respiration and dissolution of iron (III)-containing clay minerals by bacteria. *Environ. Sci. Technol.* **33,** 3127–3133.

Langley S. and Beveridge T. J. (1999) Effect of O-side-chain lipopolysaccharide chemistry on metal binding. *Appl. Environ. Microbiol.* **65,** 489–498.

Lewis D. L. and Gattie D. K. (1990) Effects of cellular aggregation on the ecology of microorganisms. *ASM News* **56,** 263–268.

Lindsay W. L. (1979) *Chemical Equilibria in Soils.* Wiley-Interscience.

Lovley D. R. and Phillips E. J. (1986a) Organic matter mineralization with reduction of ferric iron in anaerobic sediments. *Appl. Environ. Microbiol.* **51,** 683–89.

Lovley D. R. and Phillips E. J. (1986b) Availability of ferric iron for microbial reduction in bottom sediments of the freshwater tidal Potomac River. *Appl. Environ. Microbiol.* **52,** 751–57.

Lovley D. R., Coates J. D., Blunt-Harris E. L., Phillips E. J. P., and Woodward J. C. (1996) Humic substances as electron acceptors for microbial respiration. *Nature* **382,** 445–448.

Lower S., Hochella M., and Beveridge T. J. (2001) Bacterial recognition of mineral surfaces: Nanoscale interactions between *Shewanella* and α-FeOOH. *Science* **292,** 1360–1363.

Mann S., Sparks N. H. C., Couling S. B., Larcombe M. C., and Frankel R. B. (1989) Crystallochemical characterization of magnetic spinels prepared from aqueous solution. *J. Chem. Soc. Faraday Trans. 1* **85,** 3033–3044.

McGill R., McEnaney B., and Smith D. C. (1976) Crystal structure of green rust formed by corrosion of cast iron. *Nature* **259,** 200–201.

Mucci A., Richard L.F., Lucotte M., and Guignard C. (2000) The differential geochemical behavior of arsenic and phosphorus in the water column and sediments of the Saguenay Fjord estuary, Canada. *Aquat. Geochem.* **6,** 293–324.

Munch J. C. and Ottow J. C. G. (1980) Preferential reduction of amorphous to crystalline iron oxides by bacterial activity. *Soil Sci.* **129,** 15–21.

Myeni S. C. B., Tokunaga T. K., and Brown G. E. Jr. (1997) Abiotic selenium redox transformations in the presence of Fe(II, III) oxides. *Science* **278,** 1106–1109.

Myers R. and Myers J. M. (1992) Localization of cytochromes to the outer membrane of anaerobically grown *Shewanella putrefaciens* MR-1. *J. Bacteriol.* **174,** 3429–3438.

Nealson K. H., Rosson R. R., and Myers C. R. (1989) Mechanisms of oxidation and reduction of manganese. In *Metal Ions and Bacteria* (eds. T. J. Beveridge and R. Doyle), pp. 838–411. Wiley.

Nealson K. H. and Saffarini D. (1994) Iron and manganese in anaerobic respiration: Environmental significance, physiology, and regulation. *Annu. Rev. Microbiol.* **48,** 311–343.

Newman D. and Kolter R. (2000) A role for excreted quinines in extracellular electron transfer. *Nature* **405,** 94–97.

Nriagu J. O. (1972) Stability of vivianite and ion-pair formation in the system $Fe_3(PO_4)_2$-H_3PO_4-H_2O. *Geochim. Cosmochim. Acta* **36,** 459–470.

Obuekwe C. O. and Westlake W. (1982) Effects of medium composition on cell pigmentation, cytochrome content and ferric iron reduction in a *Pseudomonas* sp. isolated from crude oil. *Can. J. Microbiol.* **28,** 989–92.

Olsen S. R. and Sommers L. E. (1982) Phosphorous. In *Methods of Soil Analysis, Part 2—Chemical and Microbiological Properties* (ed. A. L. Page et al), pp. 403–430. Am. Soc. Agron.

Parmar N., Gorby Y. A., Beveridge T. J., and Ferris F. G. (2001) Formation of green rust and immobilization of nickel in response to bacterial reduction of hydrous ferric oxide. *Geomicrobiol. J.* **18,** 375–385.

Refait P. and Génin J. M. R. (1993) The oxidation of Fe(II) hydroxide in chloride-containing aqueous media and Pourbaix diagrams of green rust I. *Corros. Sci.* **34,** 797–819.

Roden E. and Zachara J. M. (1996) Microbial reduction of crystalline iron (III) oxides: Influence of oxide surface area and potential for cell growth. *Environ. Sci. Technol.* **30,** 1618–1628.

Scherer M. M., Balko B. A., and Trarnyek P. G. (1999) The role of oxides in reduction reactions at the metal–water interface. In *Mineral–Water Interfacial Reactions: Kinetics and Mechanisms* (eds. D. L. Sparks and T. J. Grundl), pp. 301–322. Symposium Series 715. American Chemical Society.

Schindler D. W. (1977) Evolution of phosphorus limitation in lakes. *Science* **195,** 260–262.

Schwertmann U. and Cornell R. M. (1991) *Iron Oxides in the Laboratory.* VCH Verlag.

Scott J. H. and Nealson K. H. (1994) A biochemical study of the intermediary carbon metabolism of *Shewanella putrefaciens. J. Bacteriol.* **176,** 3408–3411.

Seeliger S., Cord-Ruwisch R., and Schink B. (1998) A periplasmic and extracellular c-type cytochrome of *Geobacter sulfurreducens* acts as a ferric iron reductase and as an electron carrier to other acceptors or to partner bacteria. *J. Bacteriol.* **180,** 3686–3691.

Segal M. G. and Sellers R. M. (1980) Reactions of solid iron(III) oxides with aqueous reducing agents. *J. Chem. Soc. Chem. Comm.* **863,** 991–993.

Smith R. M. and Martell A. E. (1976) *Critical Stability Constants: Inorganic Complexes* Vol. 4. Plenum Press.

Sørensen J. and Jørgensen B. G. (1987) Early diagenesis in sediments from Danish coastal waters: Microbial activity and Mn-Fe-S geochemistry. *Geochim. Cosmochim. Acta* **51,** 1583–1590.

Stamatakis M. G. and Koukouzas N. K. (2001) The occurrence of phosphate minerals in lacustrine clayey diatomite deposits, Thessaly, Central Greece. *Sediment. Geol.* **139,** 33–47.

Stone A. T. and Ulrich H. J. (1989) Kinetics and reaction stoichiometry in the reductive dissolution of manganese (IV) dioxide and Co(III) oxide by hydroquinone. *J. Coll. Int. Sci.* **132,** 509–515.

Stookey L. L. (1970) Ferrozine—A new spectrophotometric reagent for iron. *Anal. Chem.* **42,** 779–781.

Stumm W. and Morgan J. (1996) *Aquatic Chemistry.* 3rd ed. Wiley Interscience.

Thamdrup B. (2000) Bacterial manganese and iron reduction in aquatic sediments. In *Advances in Microbial Ecology,* Schink B., ed. Vol. 16, pp. 41–83.

Thamdrup B. and Canfield D. E. (1996) Pathways of carbon oxidation in continental margin sediments off central Chile. *Limnol. Oceanogr.* **41,** 1629–1650.

Vargas M., Kashefi K. K., Blunt-Harris E. L., and Lovley D. R. (1998) Microbiological evidence for Fe(III) reduction on early Earth. *Nature* **395,** 65–67.

Weidler P. G., Degovics G., and Laggner P. (1998) Surface roughness created by acidic dissolution of synthetic goethite monitored with SAXS, and N_2-adsorption isotherms. *J. Colloid Interface Sci.* **197,** 1–8.

Wu J., Sunda W., Boyle E. A., and Karl D. M. (2000) Phosphate depletion in the western North Atlantic Ocean. *Science* **299,** 759–762.

Zachara J. M., Fredrickson J. K., Li S., Kennedy D. W., Smith S. C., and Gassman P. L. (1998) Bacterial reduction of crystalline Fe^{3+} oxides in single phase suspensions and subsurface materials. *Am. Mineral.* **83,** 1426–1443.